

Addressing the Readout Problem in Quantum Differential Equation Algorithms with Quantum Scientific Machine Learning

Chelsea A. Williams,^{1,2} Stefano Scali,¹ Antonio A. Gentile,² Daniel Berger,³ and Oleksandr Kyriienko^{1,2}

¹*Department of Physics and Astronomy, University of Exeter, Stocker Road, Exeter EX4 4QL, United Kingdom*

²*PASQAL, 7 Rue Léonard de Vinci, 91300 Massy, France*

³*Siemens AG, Gleiwitzer Str. 555, 90475 Nürnberg, Germany*

(Dated: November 22, 2024)

Quantum differential equation solvers aim to prepare solutions as n -qubit quantum states over a fine grid of $O(2^n)$ points, surpassing the linear scaling of classical solvers. However, unlike classically stored vectors of solutions, the readout of exact quantum states poses a bottleneck due to the complexity of tomography. Here, we show that the readout problem can be addressed with quantum learning tools where we focus on distilling the relevant features. Treating outputs of quantum differential equation solvers as quantum data, we demonstrate that low-dimensional output can be extracted using a measurement operator adapted to detect relevant features. We apply this quantum scientific machine learning approach to classify solutions for shock wave detection and turbulence modeling in scenarios where data samples come directly from quantum differential equation solvers. We show that the basis chosen for performing analysis greatly impacts classification accuracy. Our work opens up the area of research where quantum machine learning for quantum datasets is inherently required.

Introduction.—Extending the algorithmic toolbox and potential application areas of quantum computing (QC) represents an ongoing challenge for the community [1, 2]. There has been significant progress in the domain of materials science [3–6], high-energy physics [7, 8], and chemistry [9–12], with potential applications in the pharmaceutical industry [13, 14]. Financial analysis [15, 16] and optimization [17] have also attracted attention. While in each case there are hard instances to calculate, the largest workload of high-performance computing comes from solving differential equations (computational fluid dynamics and alike), reaching exascale [18–20]. This makes scientific computing an important target area for quantum algorithmic speed-up [21].

Motivated by the proposals for quantum linear solvers and the HHL algorithm [22, 23], various QC-based solvers for partial differential equations (PDEs) have been developed [24–29], and expanded to linear combination of unitaries (LCU)-based solvers [30, 31], quantum signal processing (QSP)-based solvers [32, 33], adiabatic approaches [34–36], quantum lattice Boltzmann methods [37–42], and quantum iterative solvers [43–47]. One important feature of all these methods is that they solve a *quantum* version of the linear equations problem (and corresponding PDEs), where the resulting solution is a quantum state of a n -qubit register. Reading out the full classical solution from these quantum states with tomography techniques in general scales exponentially with system size, making it prohibitive [48]. Shadow tomography is an appropriate technique for some cases but for generic solutions to PDEs, the quantum states can be entangled and complicated to process with a large shadow norm [49–51]. This represents the readout problem for quantum linear algebra algorithms [52]. While noted early on and discussed in the original HHL paper [22], the proposed mitigation to the readout problem is in measuring *some* k -local observable. This implies an understanding of what shall be measured. In fact, measuring certain observables can remove the exponential quantum advantage gained from inverting the PDE [53]. Extracting quan-

ties such as principal components or high-order statistics can be done efficiently [54] but do not always correspond to the required information. Therefore, the readout problem represents an open challenge for useful scientific computing on quantum devices.

Quantum machine learning (QML) aims to build tailored quantum circuits for analyzing data on quantum computers [52, 55]. Over the years the target of QML evolved from reaching a computational advantage in analyzing Big Data [56–58], being a distant goal due to the classical data loading bottleneck [59, 60], to the optimization-based search of optimal measurement strategies in feature spaces [61–63]. Based on adaptive circuit compilation, potential benefits of QML model building include largely increased model expressivity [62, 64, 65] and quantum-native sampling that favors generative modeling [66–72]. Applied to the domain of scientific computing, quantum scientific machine learning (QuaSciML) has emerged as a subfield of QML for solving problems based on differential equations via physics-informed modeling [73–79]. For models based on parametrized measurements this, by design, relaxes strict conditions for reading out the solutions and handling nonlinear terms [69, 73]. However QML-based modeling meets hurdles in the variational search, as trainability competes with expressivity [80].

While overcoming barren plateaus [81, 82] remains a challenge addressed from different angles [83–87], one mode of operation has emerged as a prime beneficiary—when QML is applied to *quantum* data [88, 89]. Quantum data represents states (density operators) prepared on quantum devices and supplied for QML-based processing (e.g. classification). This naturally favors QML in cases where shadow tomography is not applicable [87], and offers drastically improved generalization [88, 90–95]. However, how to get and distribute quantum data sets from physical experiments remains a puzzle.

In this work, we propose to address the readout problem of quantum differential equation solvers by using them as a source of quantum data. We demonstrate how a QuaSciML

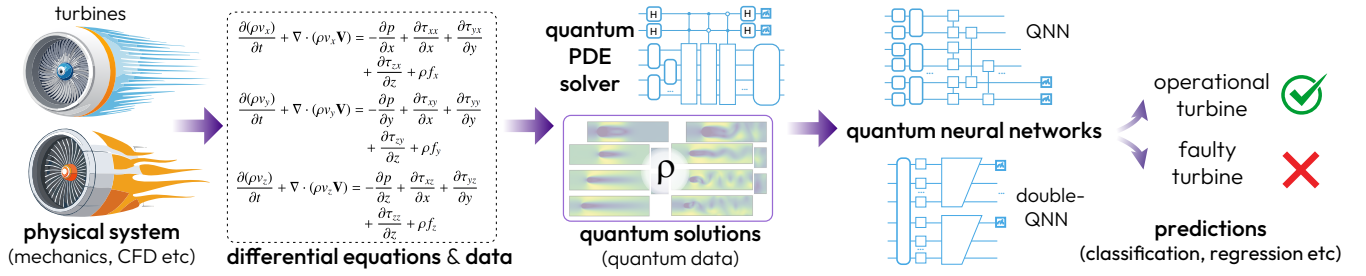


FIG. 1. A quantum CFD pipeline that uses a combination of physics-based modeling (stress, pressure, etc.) and ML to predict the behavior of an underlying system. The physics of the system is modeled by a set of PDEs that are solved with a quantum PDE solver. The quantum solutions ρ from the solver are then read out with a QuaSciML model that uses a trainable observable parametrized by a QNN to make predictions.

workflow can be adopted for classifying quantum solutions from PDE solvers, and learning relevant features (unlike plotting full solutions). Specifically, we show results from two CFD problems: the classification of wave solutions obtained from the Burgers equation, and flow regimes from the Navier-Stokes equations. These results show how QuaSciML can extract relevant information, build a problem-specific measurement operator, and highlight the influence of the chosen basis when analyzing solutions.

We note that within the field of CFD, machine learning (ML) for classification is successfully adopted, motivating the exploration of QuaSciML capabilities. For example, convolutional neural networks (CNNs) were applied to enhance turbulence modeling by distinguishing between laminar and turbulent flow regimes [96, 97] as well as being used for identifying shock wave refractions in magnetohydrodynamics [98]. This provides a way of automatically detecting points at which the solutions of the underlying PDEs become unsteady, improving the robustness of CFD pipelines. Despite these benefits, ML is limited to working with classical data (PDE solutions), and QuaSciML opens a route for analyzing large-scale CFD problems on ever-increasing grids.

Quantum Scientific Machine Learning.—Scientific machine learning (SciML) integrates data-driven models with physics-informed numerical methods to efficiently solve complex equations [99–101]. Solving PDEs with SciML requires learning a model $F : f(\mathbf{x}) \mapsto \mathbf{x}$ to extract a solution $f(\mathbf{x})$ given data \mathbf{x} [73, 77, 102, 103]. This process can get a speed-up from quantum PDE solvers [32, 44, 103, 104], where the solutions are stored as quantum states, $f(\mathbf{x}_i) \mapsto |f_i\rangle$. Thus, we arrive at the bottleneck where reading out full-grid solutions is difficult.

Addressing the readout problem requires building an efficient model to learn from quantum data, and identifying a few relevant features from complicated states. Let us thus describe the QuaSciML workflow for extracting information. Consider an input space \mathcal{X} representing the set of D quantum solutions at a grid of points $\rho = \{|f_i\rangle\}_{i=1}^D$ obtained from a quantum PDE solver and an output space \mathcal{Y} wherein classification labels are mapped. Note that the solution to the PDE f is dependent on the boundary conditions and physical variables of the under-

lying system, which ultimately influences the class that f is assigned to.

QuaSciML models can be described formally following the idea of probabilistic concepts [105]. A concept c represents a function that maps input data $\mathbf{x} \in \mathcal{X}$ to associated measured outcomes $y \in \mathcal{Y}$ such that $c : \mathcal{X} \mapsto \mathcal{Y}$. Within the context of QML, a probabilistic concept represents a quantum model that accounts for the probabilistic nature of measurements. The goal is to learn from quantum data, assigning a concept to data stored in the Hilbert space such that $c_i : |f_i\rangle \mapsto \{0, 1\} \forall i \in [1, D]$. This framework is used for developing a learning concept that is based upon parameterized quantum models. The learning algorithm seeks to minimize a loss function $L_\theta = |h(\rho, \theta) - c(\rho)|^2$ to construct a hypothesis $h(\rho, \theta)$, parameterized by θ , that approximates the true concept $c(\rho)$. The hypothesis can be developed through a variational approach or by employing a physics-informed approach that selects the optimal hypothesis from a set of measured observables representing the concept [95, 106].

The workflow of how QuaSciML can be used within the wider context of a quantum CFD pipeline is shown in Fig. 1. In terms of the quantum readout problem, the solutions (quantum states ρ) from a quantum PDE solver can be directly passed into a QuaSciML model for concept learning. The model then utilizes a parameterized quantum neural network (QNN) circuit $U(\theta)|\rho\rangle$ to extract key local and global characteristics from the quantum states. One suitable choice here is the quantum convolutional neural network (QCNN) architecture [84, 92, 107–112], which is trainable and enables a local readout. We also note that QCNNs can be treated in the measure-first form without variational training on QC in the adaptive way [87, 113], but as we work on quantum data there is still a need to identify an optimal quantum readout. Upon completing the training stage, the model learns to distinguish features such that the optimal hypothesis $h^*(\rho, \theta)$ is selected to later make informative predictions with regards to the underlying system modeled by the PDEs. In terms of quantum advantage, it has been shown that QML models can learn from exponentially fewer quantum experiments when compared with the number required by classical models [114]. The goal is to establish QuaSciML models that achieve high

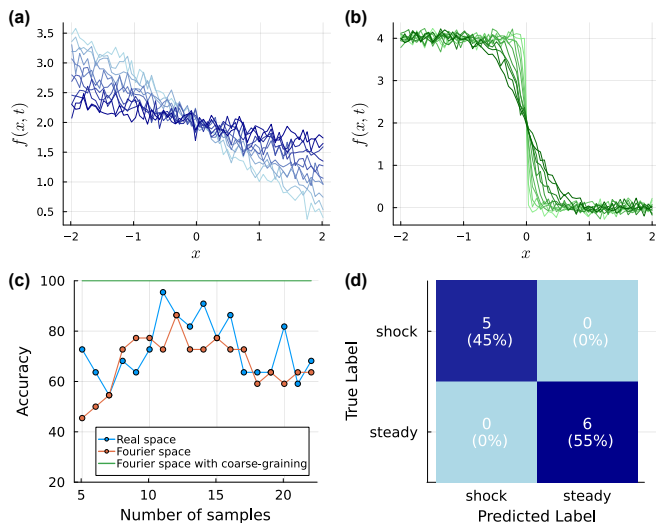


FIG. 2. The classification of wave solutions with a DQNN. **(a-b)** The one-dimensional solutions $f(x, t)$ obtained from the simulation of the Burgers equation with additional white noise. These solutions are used to classify wave behavior in terms of a steady wave (blue, left) or shock wave (green, right). Different color intensities correspond to different $t \in [0.001, 590]$ snapshots. These solutions are subsequently encoded into 6-qubit quantum states. **(c)** A comparison of the trained model accuracy as a function of the number of training samples for three DQNN models, accounting for basis choice and coarse-graining. **(d)** The confusion matrix was evaluated on a 50% test set using the optimal model that applies coarse-graining to Fourier-transformed data.

performance for PDE solutions at growing n .

The aim is to perform classification on quantum data using QNNs, optimizing a layered quantum circuit $U(\theta)$ that informs the choice of hypothesis $h(\rho, \theta)$, for constructing a sharp decision boundary. The model output is a binary label that describes CFD simulation solutions, e.g. the type of wave detected or the category of flow behavior, without needing to directly extract information from the quantum state solutions $|f\rangle$. In particular, optimized models containing problem-specific characteristics are proposed that help to inform the decision boundary and enhance the model’s accuracy through the loss minimization, $\min_{\theta}(L_{\theta})$.

Oftentimes, the optimal basis used for solving PDEs differs from the optimal basis used for learning from quantum data. In this sense, the quantum data ρ obtained from a quantum PDE solver may benefit from a basis change when uploaded to the quantum architecture used for classification. Different architectures for learning can benefit from basis changes as there can be preferred bases for performing analysis (e.g. momentum space analysis for translationally invariant solutions), influencing the ability of the model to learn the optimal concept. In composing quantum models for classification, considerations are made with regards to the basis (real space vs. Fourier space), the circuit architecture (deep-learning inspired neural networks [115] vs. convolutional neural networks [90, 92, 107]), the introduction of a coarse-grained

representation as well as common ML characteristics like the hypothesis function and optimization strategy. Here, coarse-graining refers to concentrating on part of the solution by discarding part of a register. This reduces the complexity of states to be analyzed, helping to focus on relevant macro features (e.g. vortices or flow trends). The quantum Fourier transform (QFT) is used conveniently to convert the quantum data from the real space to the Fourier space [48, 69] with an $O(n^2)$ circuit. Coarse-graining is applied afterwards to half of the register to reduce the dimensionality of the data while retaining high-frequency components of the solutions. The modified quantum data set is then fed into the model for training.

Results.—This section presents the application of the QuaSciML protocol for the purposes of binary classification. The results demonstrate the training and testing of two different quantum architectures to distinguish two fluid phenomena relevant to CFD, namely shock wave detection and turbulence modeling. For simplicity in exhibiting how the quantum read-out classification is performed, the solutions used for training and testing are obtained from classical simulations. These solutions are converted into quantum states and used as inputs to the QuaSciML models. The results from the analysis presented here are the same as if the quantum data inputs were measured directly from a noiseless quantum PDE solver without any classical processing. Therefore, the quantum data ρ represent the vectors encoding the quantum state PDE solutions in a given basis.

The first problem considers *shock wave detection* from solving the one-dimensional Burgers equation. This is a non-linear PDE that describes the propagation of waves in fluid dynamics and can be used to model various physical phenomena such as turbulence and acoustic wave propagation. The Burgers equation is given by

$$\frac{\partial f}{\partial t} + f \frac{\partial f}{\partial x} = \mu \frac{\partial^2 f}{\partial x^2}, \quad (1)$$

where μ represents the diffusivity of the medium. For this particular problem, the goal is to classify wave solutions into either shock waves or steady waves. These solutions $f(x, t)$ are shown in Fig. 2(a-b), where each solution represents a wave profile drawn at different snapshot times t . The state space is composed of 22 solutions; 11 steady wave solutions and 11 shock wave solutions. These solutions are obtained from the analytical solution to the Burgers equation using similarity transformations. Additional white noise has been added to these solutions to increase the intricacy of the profiles and subsequently enhance the complexity of the learning task.

To perform the wave behavior classification, the labeled solution set is randomly split into a training and testing set. The solutions are uploaded into quantum states using amplitude encoding, where each state is represented by 12 qubits. The model for this problem uses a deep quantum neural network (DQNN) [115] of depth 4 with an optimization procedure that consists of 300 gradient descent iterations at a learning rate of 0.05 and a hypothesis function given by the Pauli

Z measurement. The learning concept is therefore built from the hypothesis $h(\rho, \theta) = \langle \rho | U^\dagger(\theta) Z U(\theta) | \rho \rangle$. The result in Fig. 2(c) shows the accuracy of the trained model for three scenarios that consider the basis choice and the influence of coarse-graining. The number of samples refers to the number of randomly selected wave solutions drawn from the original data set for training the model, while accuracy indicates how effectively the model predicts outcomes for the entire data set.

Given the nature of this problem, it makes sense to solve the underlying differential equation in real space, as discontinuities in the solution could lead to Gibbs phenomena when using a Fourier-based approach. However, when it comes to extracting features of quantum solutions for classification, real space might not be the most suitable basis for learning. The optimal model uses a Fourier basis and a coarse-grained representation, which is shown to consistently achieve 100% accuracy. This optimized model was then applied to the full data set when split into a 50% training and 50% testing set. The confusion matrix as applied to the test set is shown in Fig. 2(d). The optimal model achieves a perfect accuracy of 100%, significantly outperforming both the real space model, which reaches only 27%, and the Fourier space model without coarse-graining, which achieves 45%. This highlights that bespoke trained models can enable efficient readout.

The second problem considers *turbulence modeling* and the solutions of two-dimensional Navier-Stokes equations. This is a set of nonlinear PDEs that describe the motion of viscous fluid flows and can be used to model various phenomena including turbulence and aerodynamics. For this particular problem, the goal is to classify the flow around a cylinder into either the laminar or turbulent regime. This is modeled by the Navier-Stokes equation,

$$\frac{\partial \mathbf{u}}{\partial t} + (\mathbf{u} \cdot \nabla) \mathbf{u} = -\frac{1}{\sigma} \nabla p + \nu \nabla^2 \mathbf{u}, \quad (2)$$

where $\mathbf{u}, \sigma, p, \nu$ respectfully represent the fluid's velocity, density, pressure, and viscosity.

The geometry of the setup is shown in Fig. 3(a), representing the flow around a cylinder. It considers the scattering of a horizontal inbound flow about a cylinder with velocity profiles modeled in the xy -plane. The two flow classes are distinguishable by their velocity profile characteristics; for laminar flows, profiles are smooth and linear while for turbulent flows, profiles are chaotic and exhibit the von Kármán vortex street phenomena. These physical features are most apparent at later stages of the flow along the x -axis, corresponding to the late-time dynamics after the flow has fully developed. To ensure that the model effectively captures these distinct dynamics, the input data is limited to the late-time behavior of the flow. This is achieved by truncating the velocity solutions to the final 25% of the flow, as indicated by the bounding box in Fig. 3(a). To reduce the dimensionality of the input data and save on computational processing time, each truncated solution is further subsampled over the coarse grid. All these steps are readily implemented for quantum data by selecting relevant qubits in the quantum register and keeping track of

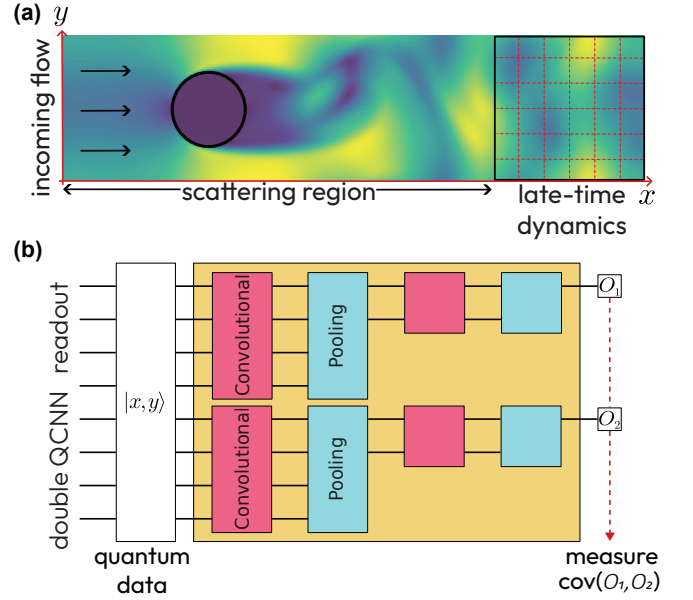


FIG. 3. The encoding of quantum data into a double-QCNN circuit for the analysis of the flow around a cylinder. (a) The geometrical configuration of the flow depicted in the xy -plane. The late-time scattering behavior of an incoming flow is subsampled from the bounded grid and encoded into the quantum state $|x, y\rangle$. (b) The quantum circuit showing the double-QCNN architecture used for the classification of two-dimensional quantum data. Each QCNN acts on a different coordinate register, parameterized by a different set of variational parameters and measured with respect to different observables $\{O_1, O_2\}$. The covariance between these observables forms the concept hypothesis and is used to learn the decision boundary.

indexing and significant bits.

The multi-dimensional nature of this problem requires encoding quantum data from grid-based inputs, necessitating that both the circuit and the model be designed to accommodate this. When uploading the solutions into quantum states with amplitude encoding, the late-time subsampled velocity arrays ψ are split across two registers. The relative quantum states are structured as

$$|\psi\rangle = |x, y\rangle = \sum_{i,j} \psi_{i,j} |i\rangle \otimes |j\rangle, \quad (3)$$

where the basis state $|i\rangle$ stores the column index corresponding to the x -register and basis state $|j\rangle$ stores the row index corresponding to the y -register. Then, two independent QNNs are applied; one on the top register and one on the bottom register. This circuit is named the double-QNN, with each network having distinct trainable parameters. The quantum circuit used to implement this strategy is given in Fig. 3(b), shown specifically for QCNNs [84, 92, 107].

Analyzing the correlation between the x -register and the y -register is an effective strategy for forming the decision boundary and devising a physics-informed hypothesis $h(\rho, \theta)$. This can be measured using covariance, where laminar solutions are expected to have a low value (approaching zero),

while turbulent solutions are likely to show a non-zero value. The covariance with respect to two operators O_1 and O_2 when measured across two different registers is given by

$$\text{cov}(O_1, O_2) = \frac{1}{2}[\langle O_1 O_2 \rangle + \langle O_2 O_1 \rangle] - \langle O_1 \rangle \langle O_2 \rangle. \quad (4)$$

The operator O_1 is measured from the top of the first register and the operator O_2 is measured from the top of the second register, as shown in Fig. 3(b). A quantum model constructed with concept learning is particularly well-suited to this problem due to the architecture's inherent ability to detect entanglement, which is crucial for analyzing correlations between different registers.

A subset of velocity solutions for different geometries and flows is shown in Fig. 4(a). Each solution represents a snapshot of the flow profile drawn at different times. The state space is composed of 200 solutions; 100 laminar flow and 100 turbulent flow solutions. These solutions are obtained with a lattice Boltzmann simulation that considers a combination of different cylinder diameters, cylinder locations along the x -axis, and variations in the collision timescale. We note that many other approaches can be adopted and here we specifically concentrate on the analysis part rather than solving. Each complete solution presented corresponds to a quantum state using 14 qubits. However, after truncating the late-time dynamics of the solution, the required number of qubits is reduced to 12. Upon further subsampling over the coarse grid, the solutions are ultimately encoded onto two registers using a total of 8 qubits.

To perform the flow behavior classification, the labeled solution set is randomly split into 75% training and 25% testing sets. The solutions correspond to quantum states with amplitude-encoded solutions that are truncated and subsampled. The model for this problem considers the QCNN [107] as the underlying architecture for the double-QNN. It incorporates a hyperbolic tangent activation function $|f\rangle \rightarrow \tanh[a(|f| - b)] \forall |f\rangle \in \rho$, where the parameters a and b are used to shift and scale the input data appropriately. The loss function is given by the covariance of the Pauli X and Pauli Z operators with an optimization procedure that consists of 100 gradient descent iterations using the parameter-shift rule at a learning rate of 0.01. The learning concept is therefore built from the hypothesis $h(\rho, \theta) = \langle \rho | U^\dagger(\theta) \text{cov}(X, Z) U(\theta) | \rho \rangle$. The result in Fig. 4(b) shows the accuracy of the trained model using a real basis, summarized over four randomly chosen seeds. As before, the number of samples refers to the number of randomly selected velocity solutions drawn from the original data set for training the model, while accuracy indicates how effectively the model predicts outcomes for the entire data set. The average confusion matrix as applied to the test set from ten randomly chosen seeds is shown in Fig. 4(c). The same analysis was performed on the model when evaluated in the Fourier basis. The QFT circuit was invoked separately on the $|x\rangle$ and $|y\rangle$ registers before applying the double-QCNN architecture. The accuracy of the trained model and average confusion matrix are shown, respectively, in Fig. 4(d) and Fig. 4(e). Although the real space model achieves a higher

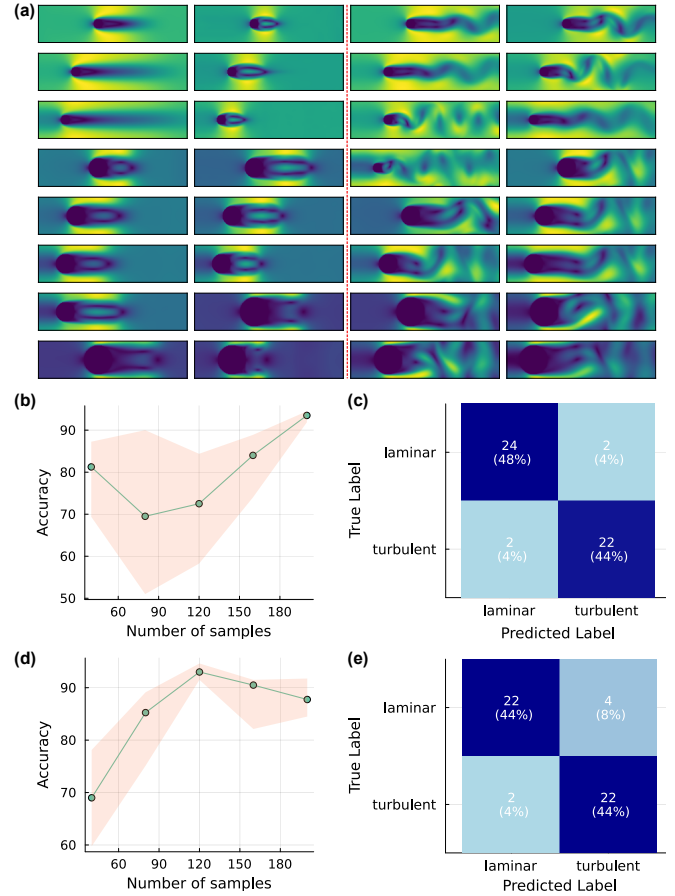


FIG. 4. The classification of flow solutions with a double-QCNN. (a) A subset of two-dimensional velocity solutions obtained from the simulation of the Navier-Stokes equations. These solutions are used to classify the flow in terms of a laminar regime (left-hand side) or turbulent regime (right-hand side). These solutions represent the amplitudes of corresponding quantum states encoded with 14 qubits. (b) The generalization (accuracy) of the trained model as a function of the training sample size for the double-QCNN model in the real basis. The line represents the median across four randomly chosen seeds and the shading denotes the inter-quartile range. (c) The confusion matrix for the double-QCNN model in the real basis, evaluated on a 25% test set as averaged across ten randomly chosen training and testing set splits. (d) Same as (b) but for the double-QCNN model in the Fourier basis. (e) Same as (c) but for the double-QCNN model in the Fourier basis.

average accuracy of 92% compared with the Fourier space model of 87%, the Fourier space model demonstrates greater stability with minimal variance in the results. The higher accuracy for the real space model makes it suitable for applications needing more precise predictions, while the Fourier space model's stability renders it more reliable in situations demanding consistent performance. In addition, the Fourier model performs better with a smaller number of samples, suggesting that the generalization and the onset of overfitting behavior differ between the two models. Overall, the optimal choice of basis for training the model will be influenced by

the trade-off between accuracy, precision, and sample size.

Conclusions.— We have shown that quantum scientific machine learning can be used as a tool for addressing the readout problem from quantum PDE solvers. By learning hypotheses as measurement operators from quantum data, one can bypass the need for computationally intensive post-processing of classical solutions extracted (e.g. tomographically) from quantum solvers. Low-dimensional output can be obtained from quantum data using models based on QNNs in the form of classification labels, representing relevant solution features, with tailored circuit architectures doing this efficiently.

The QuaSciML tools were applied to CFD problems of shock wave detection and turbulence modeling in scenarios where data samples come directly from quantum PDE solvers. We find that the proposed approach can achieve perfect scores for shockwave detection and high accuracy (> 90%) for turbulent flow detection at high test/train split ratios. We note that the success of learning depends on problem-specific characteristics and the chosen basis. Well-crafted choices in the problem representation can also considerably reduce the required resources.

Our work opens up the area of research where QuaSciML is inherently required as a quantum-enhanced post-processing step. The solutions obtained from quantum differential equation solvers will provide an abundance of quantum data (particularly, when fault-tolerant QC is available) that can be meaningfully classified. Extracting insights from these quantum solutions is a fundamental research question that we begin addressing here, with a long-term pursuit of efficient learning protocols.

Acknowledgment.—This work was supported by Siemens Industry Software NV.

-
- [1] A. Montanaro, *npj Quantum Information* **2**, 15023 (2016).
- [2] A. M. Dalzell, S. McArdle, M. Berta, P. Bienias, C.-F. Chen, A. Gilyén, C. T. Hann, M. J. Kastoryano, E. T. Khabiboulline, A. Kubica, G. Salton, S. Wang, and F. G. S. L. Brandão, Quantum algorithms: A survey of applications and end-to-end complexities (2023), [arXiv:2310.03011 \[quant-ph\]](https://arxiv.org/abs/2310.03011).
- [3] R. Babbush, N. Wiebe, J. McClean, J. McClain, H. Neven, and G. K.-L. Chan, *Phys. Rev. X* **8**, 011044 (2018).
- [4] K. J. Satzinger, Y.-J. Liu, A. Smith, C. Knapp, M. Newman, C. Jones, Z. Chen, C. Quintana, X. Mi, A. Dunsworth, C. Gidney, I. Aleiner, F. Arute, K. Arya, J. Atalaya, *et al.*, *Science* **374**, 1237 (2021), <https://www.science.org/doi/pdf/10.1126/science.abi8378>.
- [5] L. Clinton, T. Cubitt, B. Flynn, F. M. Gambetta, J. Klassen, A. Montanaro, S. Piddock, R. A. Santos, and E. Sheridan, *Nature Communications* **15**, 211 (2024).
- [6] Y. Alexeev *et al.*, *Future Generation Computer Systems* **160**, 666 (2024).
- [7] A. Di Meglio, K. Jansen, I. Tavernelli, C. Alexandrou, S. Arunachalam, C. W. Bauer, K. Borrás, S. Carrazza, A. Crippa, V. Croft, R. de Putter, A. Delgado, V. Dunjko, D. J. Egger, E. Fernández-Combarro, *et al.*, *PRX Quantum* **5**, 037001 (2024).
- [8] J. J. Martínez de Lejarza, L. Cieri, M. Grossi, S. Vallecorsa, and G. Rodrigo, *Phys. Rev. D* **110**, 074031 (2024).
- [9] S. McArdle, S. Endo, A. Aspuru-Guzik, S. C. Benjamin, and X. Yuan, *Rev. Mod. Phys.* **92**, 015003 (2020).
- [10] Y. Cao, J. Romero, J. P. Olson, M. Degroote, P. D. Johnson, M. Kieferová, I. D. Kivlichan, T. Menke, B. Peropadre, N. P. Sawaya, *et al.*, *Chemical reviews* **119**, 10856 (2019).
- [11] J. Lee, D. W. Berry, C. Gidney, W. J. Huggins, J. R. McClean, N. Wiebe, and R. Babbush, *PRX Quantum* **2**, 030305 (2021).
- [12] J. Robledo-Moreno, M. Motta, H. Haas, A. Javadi-Abhari, P. Jurcevic, W. Kirby, S. Martiel, K. Sharma, S. Sharma, T. Shirakawa, I. Sitdikov, R.-Y. Sun, K. J. Sung, M. Takita, M. C. Tran, *et al.*, *Chemistry beyond exact solutions on a quantum-centric supercomputer* (2024), [arXiv:2405.05068 \[quant-ph\]](https://arxiv.org/abs/2405.05068).
- [13] R. Santagati, A. Aspuru-Guzik, R. Babbush, M. Degroote, L. González, E. Kyoseva, N. Moll, M. Oppel, R. M. Parrish, N. C. Rubin, M. Streif, C. S. Tautermann, H. Weiss, N. Wiebe, and C. Utschig-Utschig, *Nature Physics* **20**, 549 (2024).
- [14] Y. Zhou, J. Chen, J. Cheng, G. Karemore, M. Zitnik, F. T. Chong, J. Liu, T. Fu, and Z. Liang, *Quantum-machine-assisted drug discovery: Survey and perspective* (2024), [arXiv:2408.13479 \[quant-ph\]](https://arxiv.org/abs/2408.13479).
- [15] D. Herman, C. Googin, X. Liu, Y. Sun, A. Galda, I. Safro, M. Pistoia, and Y. Alexeev, *Nature Reviews Physics* **5**, 450 (2023).
- [16] P. Mironowicz, A. S. H., A. Mandarino, A. E. Yilmaz, and T. Ankenbrand, *Applications of quantum machine learning for quantitative finance* (2024), [arXiv:2405.10119 \[quant-ph\]](https://arxiv.org/abs/2405.10119).
- [17] A. Abbas, A. Ambainis, B. Augustino, A. Bärttschi, H. Buhman, C. Coffrin, G. Cortiana, V. Dunjko, D. J. Egger, B. G. Elmegreen, N. Franco, F. Fratini, B. Fuller, J. Gacon, C. Gocialea, *et al.*, *Nature Reviews Physics* **10.1038/s42254-024-00770-9** (2024).
- [18] S. Heldens, P. Hijma, B. V. Werkhoven, J. Maassen, A. S. Z. Belloum, and R. V. Van Nieuwpoort, *ACM Comput. Surv.* **53**, 10.1145/3372390 (2020).
- [19] P. Mullaney, R. Li, S. Thomas, S. Ananthan, A. Sharma, J. S. Rood, A. B. Williams, and M. A. Sprague, in *Proceedings of the International Conference for High Performance Computing, Networking, Storage and Analysis, SC '21* (Association for Computing Machinery, New York, NY, USA, 2021).
- [20] C. Coti, Y. Pfau-Kempf, M. Battarbee, U. Ganse, S. Shende, K. Huck, J. Rodriguez, L. Kotipalo, J. Faj, J. J. Williams, I. Peng, A. D. Malony, S. Markidis, and M. Palmroth, in *2024 IEEE International Parallel and Distributed Processing Symposium Workshops (IPDPSW)* (2024) pp. 996–1005.
- [21] M. Möller, Quantum scientific computing, in *Impact of Scientific Computing on Science and Society*, edited by P. Neittaanmäki and M.-L. Rantalainen (Springer International Publishing, Cham, 2023) pp. 357–371.
- [22] A. W. Harrow, A. Hassidim, and S. Lloyd, *Physical review letters* **103**, 150502 (2009).
- [23] A. Martin, R. Ibarrondo, and M. Sanz, *Phys. Rev. Appl.* **19**, 064056 (2023).
- [24] D. W. Berry, *Journal of Physics A: Mathematical and Theoretical* **47**, 105301 (2014).
- [25] A. Montanaro and S. Pallister, *Phys. Rev. A* **93**, 032324 (2016).
- [26] P. C. S. Costa, S. Jordan, and A. Ostrander, *Phys. Rev. A* **99**, 012323 (2019).
- [27] A. Scherer, B. Valiron, S.-C. Mau, S. Alexander, E. van den Berg, and T. E. Chapuran, *Quantum Information Processing* **16**, 60 (2017).

- [28] H. Krovi, *Quantum* **7**, 913 (2023).
- [29] B. Daribayev, A. Mukhanbet, and T. Imankulov, *Applied Sciences* **13**, 10.3390/app132011491 (2023).
- [30] A. M. Childs, R. Kothari, and R. D. Somma, *SIAM Journal on Computing* **46**, 1920 (2017).
- [31] A. M. Childs and N. Wiebe, *Quantum Info. Comput.* **12**, 901–924 (2012).
- [32] L. Lin and Y. Tong, *Quantum* **4**, 361 (2020).
- [33] J. M. Martyn, Z. M. Rossi, A. K. Tan, and I. L. Chuang, *PRX Quantum* **2**, 040203 (2021).
- [34] Y. Subaşı, R. D. Somma, and D. Orsucci, *Physical Review Letters* **122**, 060504 (2019).
- [35] P. C. S. Costa, P. Schleich, M. E. S. Morales, and D. W. Berry, Further improving quantum algorithms for nonlinear differential equations via higher-order methods and rescaling (2023), [arXiv:2312.09518 \[quant-ph\]](https://arxiv.org/abs/2312.09518).
- [36] D. Jennings, M. Lostaglio, S. Pallister, A. T. Sornborger, and Y. Subaşı, Efficient quantum linear solver algorithm with detailed running costs (2023), [arXiv:2305.11352 \[quant-ph\]](https://arxiv.org/abs/2305.11352).
- [37] S. Succi, F. Fillion-Gourdeau, and S. Palpacelli, *EPJ Quantum Technology* **2**, 12 (2015).
- [38] R. Steijl, *Applied Sciences* **13** (2023).
- [39] M. A. Schalkers and M. Möller, Efficient and fail-safe collisionless quantum boltzmann method (2022), [arXiv:2211.14269 \[quant-ph\]](https://arxiv.org/abs/2211.14269).
- [40] M. A. Schalkers and M. Möller, On the importance of data encoding in quantum boltzmann methods (2023), [arXiv:2302.05305 \[quant-ph\]](https://arxiv.org/abs/2302.05305).
- [41] S. Succi, W. Itani, K. Sreenivasan, and R. Steijl, *Europhysics Letters* **144**, 10001 (2023).
- [42] S. Succi, W. Itani, C. Sanavio, K. R. Sreenivasan, and R. Steijl, *Computers & Fluids* **270**, 106148 (2024).
- [43] C. Shao and H. Xiang, *Physical Review A* **101** (2020).
- [44] C. A. Williams, A. A. Gentile, V. E. Elfving, D. Berger, and O. Kyriienko, *Quantum iterative methods for solving differential equations with application to computational fluid dynamics* (2024), [arXiv:2404.08605 \[quant-ph\]](https://arxiv.org/abs/2404.08605).
- [45] O. M. Raisuddin and S. De, Quantum relaxation method for linear systems in finite element problems (2023), [arXiv:2308.01377 \[quant-ph\]](https://arxiv.org/abs/2308.01377).
- [46] O. M. Raisuddin and S. De, Quantum multigrid algorithm for finite element problems (2024), [arXiv:2404.07466 \[quant-ph\]](https://arxiv.org/abs/2404.07466).
- [47] S. Jin and N. Liu, Quantum simulation of discrete linear dynamical systems and simple iterative methods in linear algebra via schrodingerisation (2023), [arXiv:2304.02865 \[quant-ph\]](https://arxiv.org/abs/2304.02865).
- [48] M. A. Nielsen and I. L. Chuang, *Quantum computation and quantum information* (Cambridge university press, 2010).
- [49] H.-Y. Huang, R. Kueng, and J. Preskill, *Nature Physics* **16**, 1050 (2020).
- [50] S. Jerbi, C. Gyurik, S. C. Marshall, R. Molteni, and V. Dunjko, *Nature Communications* **15**, 5676 (2024).
- [51] Y. Zhou and Z. Liu, *A hybrid framework for estimating nonlinear functions of quantum states* (2023), [arXiv:2208.08416 \[quant-ph\]](https://arxiv.org/abs/2208.08416).
- [52] J. Biamonte, P. Wittek, N. Pancotti, P. Rebentrost, N. Wiebe, and S. Lloyd, *Nature* **549**, 195 (2017).
- [53] N. Linden, A. Montanaro, and C. Shao, *Communications in Mathematical Physics* **395**, 601 (2022).
- [54] S. Lloyd, M. Mohseni, and P. Rebentrost, *Nature Physics* **10**, 631 (2014).
- [55] M. Benedetti, E. Lloyd, S. Sack, and M. Fiorentini, *Quantum Science and Technology* **4**, 043001 (2019).
- [56] N. Wiebe, D. Braun, and S. Lloyd, *Phys. Rev. Lett.* **109**, 050505 (2012).
- [57] P. Rebentrost, M. Mohseni, and S. Lloyd, *Phys. Rev. Lett.* **113**, 130503 (2014).
- [58] M. Schuld, I. Sinayskiy, and F. Petruccione, *Phys. Rev. A* **94**, 022342 (2016).
- [59] M. Schuld and N. Killoran, *PRX Quantum* **3**, 030101 (2022).
- [60] M. Cerezo, G. Verdon, H.-Y. Huang, L. Cincio, and P. J. Coles, *Nature Computational Science* **2**, 567 (2022).
- [61] M. Schuld and N. Killoran, *Phys. Rev. Lett.* **122**, 040504 (2019).
- [62] T. Goto, Q. H. Tran, and K. Nakajima, *Phys. Rev. Lett.* **127**, 090506 (2021).
- [63] M. Schuld, Supervised quantum machine learning models are kernel methods (2021), [arXiv:2101.11020 \[quant-ph\]](https://arxiv.org/abs/2101.11020).
- [64] M. Schuld, R. Sweke, and J. J. Meyer, *Phys. Rev. A* **103**, 032430 (2021).
- [65] A. Abbas, D. Sutter, C. Zoufal, A. Lucchi, A. Figalli, and S. Woerner, *Nature Computational Science* **1**, 403 (2021).
- [66] J.-G. Liu and L. Wang, *Phys. Rev. A* **98**, 062324 (2018).
- [67] C. Zoufal, A. Lucchi, and S. Woerner, *npj Quantum Information* **5**, 103 (2019).
- [68] B. Coyle, D. Mills, V. Danos, and E. Kashefi, *npj Quantum Information* **6**, 60 (2020).
- [69] O. Kyriienko, A. E. Paine, and V. E. Elfving, *Phys. Rev. Res.* **6**, 033291 (2024).
- [70] S. Kasture, O. Kyriienko, and V. E. Elfving, *Phys. Rev. A* **108**, 042406 (2023).
- [71] M. S. Rudolph, S. Lerch, S. Thanasilp, O. Kiss, O. Shaya, S. Vallecorsa, M. Grossi, and Z. Holmes, *npj Quantum Information* **10**, 116 (2024).
- [72] H.-Y. Wu, V. E. Elfving, and O. Kyriienko, *Advanced Quantum Technologies* , 2400337 (2024), <https://onlinelibrary.wiley.com/doi/pdf/10.1002/qute.202400337>.
- [73] O. Kyriienko, A. E. Paine, and V. E. Elfving, *Physical Review A* **103**, 052416 (2021).
- [74] N. Heim, A. Ghosh, O. Kyriienko, and V. E. Elfving, Quantum model-discovery (2021), [arXiv:2111.06376 \[quant-ph\]](https://arxiv.org/abs/2111.06376).
- [75] S. Markidis, *Frontiers in Applied Mathematics and Statistics* **8** (2022).
- [76] A. E. Paine, V. E. Elfving, and O. Kyriienko, *Advanced Quantum Technologies* **6**, 2300065 (2023).
- [77] A. E. Paine, V. E. Elfving, and O. Kyriienko, *Physical Review A* **107**, 032428 (2023).
- [78] B. Jaderberg, A. A. Gentile, Y. A. Berrada, E. Shishenina, and V. E. Elfving, *Phys. Rev. A* **109**, 042421 (2024).
- [79] B. Jaderberg, A. A. Gentile, A. Ghosh, V. E. Elfving, C. Jones, D. Vodola, J. Manobianco, and H. Weiss, *Phys. Rev. A* **110**, 052423 (2024).
- [80] Z. Holmes, K. Sharma, M. Cerezo, and P. J. Coles, *PRX Quantum* **3**, 010313 (2022).
- [81] J. R. McClean, S. Boixo, V. N. Smelyanskiy, R. Babbush, and H. Neven, *Nature communications* **9**, 4812 (2018).
- [82] E. Fontana, D. Herman, S. Chakrabarti, N. Kumar, R. Yalovetzky, J. Heredge, S. H. Sureshbabu, and M. Pistoia, The adjoint is all you need: Characterizing barren plateaus in quantum ansätze (2023), [arXiv:2309.07902 \[quant-ph\]](https://arxiv.org/abs/2309.07902).
- [83] S. H. Sack, R. A. Medina, A. A. Michailidis, R. Kueng, and M. Serbyn, *PRX Quantum* **3**, 020365 (2022).
- [84] A. Pesah, M. Cerezo, S. Wang, T. Volkoff, A. T. Sornborger, and P. J. Coles, *Physical Review X* **11**, 041011 (2021).
- [85] M. Larocca, N. Ju, D. García-Martín, P. J. Coles, and M. Cerezo, *Nature Computational Science* **3**, 542 (2023).
- [86] R. Puig, M. Drudis, S. Thanasilp, and Z. Holmes, *Variational quantum simulation: a case study for understanding warm starts* (2024), [arXiv:2404.10044 \[quant-ph\]](https://arxiv.org/abs/2404.10044).

- [87] M. Cerezo, M. Larocca, D. García-Martín, N. L. Diaz, P. Braccia, E. Fontana, M. S. Rudolph, P. Bermejo, A. Ijaz, S. Thanasilp, E. R. Anschuetz, and Z. Holmes, Does provable absence of barren plateaus imply classical simulability? or, why we need to rethink variational quantum computing (2023), [arXiv:2312.09121 \[quant-ph\]](https://arxiv.org/abs/2312.09121).
- [88] H.-Y. Huang, M. Broughton, J. Cotler, S. Chen, J. Li, M. Mohseni, H. Neven, R. Babbush, R. Kueng, J. Preskill, and J. R. McClean, *Science* **376**, 1182 (2022).
- [89] M. Cerezo, G. Verdon, H.-Y. Huang, L. Cincio, and P. J. Coles, *Nature Computational Science* **2**, 567 (2022).
- [90] M. C. Caro, H.-Y. Huang, M. Cerezo, K. Sharma, A. Sornborger, L. Cincio, and P. J. Coles, *Nature Communications* **13**, 4919 (2022).
- [91] M. C. Caro, H.-Y. Huang, N. Ezzell, J. Gibbs, A. T. Sornborger, L. Cincio, P. J. Coles, and Z. Holmes, *Nature Communications* **14**, 3751 (2023).
- [92] C. Umeano, A. E. Paine, V. E. Elfving, and O. Kyriienko, What can we learn from quantum convolutional neural networks? (2023), [arXiv:2308.16664 \[quant-ph\]](https://arxiv.org/abs/2308.16664).
- [93] E. Gil-Fuster, J. Eisert, and C. Bravo-Prieto, Understanding quantum machine learning also requires rethinking generalization (2023), [arXiv:2306.13461 \[quant-ph\]](https://arxiv.org/abs/2306.13461).
- [94] C. Umeano, V. E. Elfving, and O. Kyriienko, *Geometric quantum machine learning of bqp^q protocols and latent graph classifiers* (2024), [arXiv:2402.03871 \[quant-ph\]](https://arxiv.org/abs/2402.03871).
- [95] C. Umeano, S. Scali, and O. Kyriienko, *Can geometric quantum machine learning lead to advantage in barcode classification?* (2024), [arXiv:2409.01496 \[quant-ph\]](https://arxiv.org/abs/2409.01496).
- [96] *Is it Turbulent or Laminar? Convolutional Neural Network Predictions*, Fluids Engineering Division Summer Meeting, Vol. Volume 2: Multiphase Flow (MFTC); Computational Fluid Dynamics (CFDTC); Micro and Nano Fluid Dynamics (MNFDTTC) (2022).
- [97] L. Deng, Y. Wang, Y. Liu, F. Wang, S. Li, and J. Liu, *J. Vis.* **22**, 65–78 (2019).
- [98] F. Chen and R. Samtaney, *Physics of Fluids* **34**, 10.1063/5.0105098 (2022).
- [99] Sciml: Open source software for scientific machine learning, <https://sciml.ai/> (2023), accessed: 30-07-2023.
- [100] C. Rackauckas, M. Innes, Y. Ma, J. Bettencourt, L. White, and V. Dixit, arXiv preprint [arXiv:1902.02376](https://arxiv.org/abs/1902.02376) (2019).
- [101] C. Rackauckas, Y. Ma, J. Martensen, C. Warner, K. Zubov, R. Supekar, D. Skinner, and A. Ramadhan, arXiv preprint [arXiv:2001.04385](https://arxiv.org/abs/2001.04385) (2020).
- [102] M. Lubasch, J. Joo, P. Moinier, M. Kiffner, and D. Jaksch, *Physical Review A* **101**, 010301 (2020).
- [103] A. E. Paine, V. E. Elfving, and O. Kyriienko, Physics-informed quantum machine learning: Solving nonlinear differential equations in latent spaces without costly grid evaluations (2023), [arXiv:2308.01827 \[quant-ph\]](https://arxiv.org/abs/2308.01827).
- [104] D. An, J.-P. Liu, D. Wang, and Q. Zhao, *A theory of quantum differential equation solvers: limitations and fast-forwarding* (2023), [arXiv:2211.05246 \[quant-ph\]](https://arxiv.org/abs/2211.05246).
- [105] B. Y. Gan, P.-W. Huang, E. Gil-Fuster, and P. Rebentrost, *Concept learning of parameterized quantum models from limited measurements* (2024), [arXiv:2408.05116 \[quant-ph\]](https://arxiv.org/abs/2408.05116).
- [106] C. Gyurik and V. Dunjko, Exponential separations between classical and quantum learners (2023), [arXiv:2306.16028 \[quant-ph\]](https://arxiv.org/abs/2306.16028).
- [107] I. Cong, S. Choi, and M. D. Lukin, *Nature Physics* **15**, 1273–1278 (2019).
- [108] J. Herrmann, S. M. Llima, A. Remm, P. Zapletal, N. A. McMahon, C. Scarato, F. Swiadek, C. K. Andersen, C. Hellings, S. Krinner, N. Lacroix, S. Lazar, M. Kerschbaum, D. C. Zanuz, G. J. Norris, *et al.*, *Nature Communications* **13**, 4144 (2022).
- [109] P. Zapletal, N. A. McMahon, and M. J. Hartmann, Error-tolerant quantum convolutional neural networks for symmetry-protected topological phases (2023), [arXiv:2307.03711 \[quant-ph\]](https://arxiv.org/abs/2307.03711).
- [110] F. Shen and J. Liu, Qfcnn: Quantum fourier convolutional neural network (2021), [arXiv:2106.10421 \[quant-ph\]](https://arxiv.org/abs/2106.10421).
- [111] K. Chinzei, Q. H. Tran, K. Maruyama, H. Oshima, and S. Sato, *Phys. Rev. Res.* **6**, 023042 (2024).
- [112] L. C. Sander, N. A. McMahon, P. Zapletal, and M. J. Hartmann, *Quantum convolutional neural network for phase recognition in two dimensions* (2024), [arXiv:2407.04114 \[quant-ph\]](https://arxiv.org/abs/2407.04114).
- [113] P. Bermejo, P. Braccia, M. S. Rudolph, Z. Holmes, L. Cincio, and M. Cerezo, *Quantum convolutional neural networks are (effectively) classically simulable* (2024), [arXiv:2408.12739 \[quant-ph\]](https://arxiv.org/abs/2408.12739).
- [114] H.-Y. Huang, M. Broughton, J. Cotler, S. Chen, J. Li, M. Mohseni, H. Neven, R. Babbush, R. Kueng, J. Preskill, and J. R. McClean, *Science* **376**, 1182–1186 (2022).
- [115] K. Beer, D. Bondarenko, T. Farrelly, T. J. Osborne, R. Salzmann, D. Scheiermann, and R. Wolf, *Nature Communications* **11** (2019).